Transitions and Relaxations of Copolypropylene Molecules in Copolypropylene–Clay Composites

Weixia Zhong, Xiuying Qiao, Ming Cao, Kang Sun, Guoding Zhang

State Key Laboratory of Metal Matrix Composites, Shanghai Jiao Tong University, Shanghai 200030, China

Received 18 November 2005; accepted 21 March 2006
DOI 10.1002/app.24489
Published online 12 October 2007 in Wiley InterScience (www.interscience.wiley.com).

ABSTRACT: Three commercial organoclays pretreated with $C_{18}H_{37}N^+H_3$, $C_{18}H_{37}N^+(CH_3)_3$ and $(C_{18}H_{37})_2N^+(CH_3)_2$, were used to prepare a series of copolypropylene (cPP)-clay nancomposites by melt blending. Then, the effects of the clay content and pretreatment history on the transition and relaxation of cPP molecules in different composites were investigated in detail by dynamic mechanical analysis. The results show that the α-relaxation, ascribed to the movement of polymer main chains within the crystalline regions of different cPP composites, is activated by the increase of clay content. The main β-relaxation, assigned to the glass-rubber transition of cPP segments in amorphous portions, is greatly limited by about 3–5 wt % clay loading, whereas drastically motivated with 7 wt % clay loading, which correlates closely with the dispersion order of clay layers in different composites. Lastly, the γ-relaxation, associated with the motion of ethylene sequence of cPP chains, is restricted because of the increasing clay content. Additionally, it is found that the miscibility between cPP molecules and organoclay layers was strengthened as the clay premodifier varied from $C_{18}H_{37}N^+H_3$ to $C_{18}H_{37}N^+(CH_3)_3$, but somewhat weakened when the premodifier changed as $(C_{18}H_{37})_2N^+(CH_3)_2$. © 2007 Wiley Periodicals, Inc. J Appl Polym Sci 107: 1407–1413, 2008

Key words: copolypropylene; clay; composite; dynamic mechanical analysis; relaxation

INTRODUCTION

In recent years, polymer–clay nanocomposites have attracted intensive attentions because of their more remarkable improvement of physical properties than that of the neat polymer and conventional composite counterparts. Polypropylene (PP)–clay nanocomposite, as one of the pioneer systems in fields of polymer nanocomposites, has been extensively studied.[1–8] Nevertheless, copolypropylene(cPP)–clay systems have been seldom mentioned. When compared with homopolypropylene, cPP has many advantages such as excellent low-temperature impact property, stable performance, high sales profits, and good transparency of the end products. By now, cPP is playing an increasingly important role in the whole PP market, widely used in injection molding, film, and fiber areas. Therefore, researches of the blending of clay into the cPP matrix would be of great significance to expand the application of cPP.

It is well known that the physical properties of a polymeric material are strongly dependent on its morphology, structure, and relaxation processes corresponding to internal changes and molecular motions.[9] Dynamic mechanical measurements over a wide temperature of frequency range are useful in understanding of the viscoelastic behavior and provide valuable insights into the relationship between structure, morphology, and applicational properties of polymers and polymer composites.[10–11] Previous studies on PP–clay composites have mentioned the influences of clay on PP glass transition temperature (T_g), dynamic modulus, and damping factor (tan δ) of composites by dynamic mechanical analysis (DMA). However, effects of clay pretreatments as well as loadings on the transitions and relaxations of polymer molecular units within different corresponding composites are never reported.

Thus, in this work, a series of cPP–clay nanocomposite (cPPCN) were prepared by melt blending three commercial organoclays (pretreated with $C_{18}H_{37}NH_3^+$, $C_{18}H_{37}N(CH_3)_3^+$, and $(C_{18}H_{37})_2N(CH_3)_2^+$) into the cPP matrix with maleic anhydride modified PP (MA-PP) as a compatibilizer. Effects of the clay pretreatment and content on the transitions and relaxations of cPP different units in these composites were detected in detail by means of DMA. The occurrence of molecular mobility transitions are discussed related to structure variations of composites. Additionally, the affinity between cPP matrix and clay layers was also estimated by calculating the activation energy of cPP moving units of different composites.

EXPERIMENTAL

Materials

The polymer matrix for the composites was copolypropylene (low ethylene content polypropylene copolymer),

Correspondence to: K. Sun (ksun@sjtu.edu.cn).

Journal of Applied Polymer Science, Vol. 107, 1407–1413 (2008)

SB9430 (MFI = 30 g/10 min, $\rho = 0.91$ g/cm^3) produced by Korea PetroChemical Ind. The compatibilizer used was maleic anhydride grafted isotactic polypropylene (MA-PP) provided by Shanghai Sunny New Technology Development Co., having 1.0% MAH content. Three commercially organophilic montmorillonite (OMMT) premodified by $C_{18}H_{37}N^+H_3$, $C_{18}H_{37}N^+(CH_3)_3$, and $(C_{18}H_{37})_2N^+(CH_3)_2$ separately were denoted as $OMMT_1$, $OMMT_2$, and $OMMT_3$, supplied by Fenghong clay, China, and their specific parameters were listed in Table I.

Preparation of cPP–clay composites

All cPP-clay composites were prepared by melt intercalation with a thermoplastic mixer of Rheocord 900 Haake. The compatibilizer content of MA-PP was kept at 21 wt %, and three organoclays were loaded at 0, 3, 5, and 7 wt %, respectively. The melt-mixed process was performed at 180°C with a rotor speed of 100 rpm for 15 min, and the abbreviations and compositions for the resulting composites were listed in Table II. Subsequently, the obtained blends were compression-molded into pieces of 100 × 100 × 1 mm^3 for the following measurements.

X-ray diffraction

The interlayer distance of the organoclay in the composites was studied at ambient temperature by using an X-ray diffractometer measurement (D/MAXIII, Japan), with a Cu Kα radiation ($\lambda = 0.154$ nm). All the samples were scanned by plates over a 2θ range of 1°–30° at a rate of 2°/min. As for these samples, the interlayer distance of organoclays were determined from the (001) reflection peak in the XRD patterns of 1°–10°, and the crystal structures of the cPP original and cPP in composites were investigated from the XRD patterns of 10°–30°.

Differential scanning calorimetry

The thermal property of PP composites was analyzed on a DSC Q10 differential scanning calorimeter thermal analyzer (TA Instruments). Test specimens (4–10 mg) were first heated from 20 to 210°C at a rate of 20°C/min and then maintained there for 5 min to eliminate the effects of preconditions. In succession, the samples were cooled down to 20°C at a rate of 10°C/min (crystallizing cycle), and after that, heated again from 20 to 210°C at a rate of 10°C/min (melting cycle). All the experiments were carried out under a nitrogen protection. From the thermograms, transition temperatures and enthalpies can be obtained and the degree of crystallinity also determined.

TABLE I
Characteristics of Three Types of Organoclay

Clay	CEC[a] (meq/100 g)	Exchanged ion	Diameter (nm)	d_{001}(m)/2θ
$OMMT_1$	110–120	$C_{18}H_{37}NH_3^+$	25,000	2.1/4.1°
$OMMT_2$	110–120	$C_{18}H_{37}N(CH_3)_3^+$	25,000	2.4/3.7°
$OMMT_3$	110–120	$(C_{18}H_{37})_2N(CH_3)_2^+$	25,000	3.7/2.4° 1.9/4.7°

[a] Cation exchange capacity, meq/100 g of clay.

TABLE II
Abbreviations and Compositions of All Samples

Sample	Compositions
cPP	cPP(100)
cPPCN0	cPP/MA-PP(79/21)
cPPCN1(3)	cPP/MA-PP/$OMMT_1$(76/21/3)
cPPCN1(5)	cPP/MA-PP/$OMMT_1$(74/21/5)
cPPCN1(7)	cPP/MA-PP/$OMMT_1$(72/21/7)
cPPCN2(3)	cPP/MA-PP/$OMMT_2$(76/21/3)
cPPCN2(5)	cPP/MA-PP/$OMMT_2$(74/21/5)
cPPCN2(7)	cPP/MA-PP/$OMMT_2$(72/21/7)
cPPCN3(3)	cPP/MA-PP/$OMMT_3$(76/21/3)
cPPCN3(5)	cPP/MA-PP/$OMMT_3$(74/21/5)
cPPCN3(7)	cPP/MA-PP/$OMMT_3$(72/21/7)

Dynamic mechanical analysis

Dynamic mechanical analysis was carried out on Rheometrics Dynamic Mechanical Analyzer (DMA IV). Test samples were bars (about 15 mm length, 4 mm width) cut from the compression-molded plaques. The DMA experiments were performed in a single-point bending mode over a wide frequency range (0.1, 1, 5 and 10 Hz) with a temperature range from −100 to 150°C and a heating rate of 3°C/min under a controlled sinusoidal strain. The viscoelastic property parameters, such as the storage modulus (E') and loss factor tan δ (tan $\delta = E'/E''$, loss modulus (E'')) were recorded as a function of temperature and frequency.

The activation energy of each relaxation process for cPP in different composites was obtained from the temperature dependence of different testing frequency on the dynamic mechanical spectra around the corresponding relaxation temperature:

$$\ln\left(\frac{f_1}{f_2}\right) = \frac{\Delta E_a}{R}\left(\frac{1}{T_2} - \frac{1}{T_1}\right)$$

where R is the gas constant (8.314 J K^{-1} mol^{-1}), ΔE_a is the activation energy for the relaxation, and T_1 and T_2 corresponds to the loss peak positions at two frequencies, f_1 and f_2.[12]

RESULTS AND DISCUSSION

Clay dispersion

The characteristics of the three virgin organoclay (i.e., $OMMT_1$, $OMMT_2$, and $OMMT_3$) are shown in Table I.

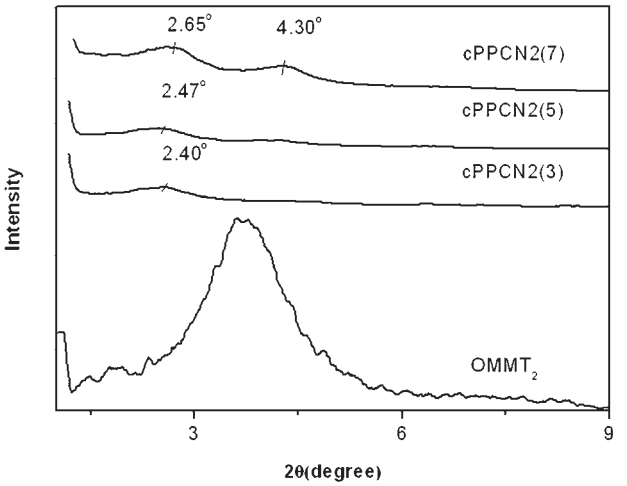

Figure 1 WAXD patterns of the virgin OMMT2 and OMMT2 in different cPP–clay composites.

Three virgin OMMTs have different average interlayer spacing (d_{001}) due to their different pretreatments with $C_{18}H_{37}NH_3^+$, $C_{18}H_{37}N(CH_3)_3^+$ and $(C_{18}H_{37})_2N(CH_3)_2^+$, respectively, and the d_{001} size follows as $OMMT_3 > OMMT_2 > OMMT_1$, as seen in Table I. After being blended with the cPP matrix, three OMMTs display different dispersion status owing to their different pretreatments.

Here, the complete WAXD patterns for the cPP-$OMMT_2$ systems with different $OMMT_2$ loadings are offered in Figure 1 to discuss the effect of clay loadings. And, effects of the OMMT pretreatments on the WAXD patterns for their composites are shown in Figure 2. As seen in Figure 1, the diffraction peak of $OMMT_2$ in composites clearly shifted to a lower diffraction angle (2θ) and appeared to be weaker and broader with respect to the pure $OMMT_2$. This variation indicates that the melt blending of $OMMT_2$ within the cPP matrix helped to increase the interlayer spacing of $OMMT_2$, simultaneously, improved the $OMMT_2$ exfoliation. Nevertheless, as the $OMMT_2$ loading increases up to 7 wt %, such an increase of the $OMMT_2$ interlayer spacing decreases and $OMMT_2$ also exhibits a weak peak at 4.3° with a layer distance of about 2.0 nm. This phenomenon indicates that $OMMT_2$ layers gradually appears an increasing jam status in cPPCN2(7), and such this jam dispersion of clay layers should be more intense in cPPCN1(7). As seen in Figure 2, the diffraction peak of $OMMT_1$ in cPPCN1(7) only located at 3.4° with a smaller d_{001} of 2.6 nm than that of 3.8 nm for $OMMT_2$ in cPPCN2(7). In cPPCN3(7), the $OMMT_3$ diffraction peak hardly changed compared with the diffraction pattern of the pure $OMMT_3$, which implies that the original structure of $OMMT_3$ in cPPCN3(7) was hardly disturbed during being melt blended with cPP molecules. The reason for this is that full of C_{18}-alkyl chains have congested between the interlayer spaces of $OMMT_3$, thus obstructing the cPP intercalation into the OMMT layers during melt blending. Therefore, among these three OMMTs, $OMMT_2$, previously modified by $C_{18}H_{37}N(CH_3)_3^+$, could be relatively better expanded and exfoliated than the two other clays within the cPP matrix, although a full exfoliation was still not achieved here.

Characteristic of cPP crystallites

WAXD studies were carried out to obtain the information on the crystalline level of cPP-clay composites, and the resultant diffraction angle (2θ) curves are given in Figure 3. Diffractions for pure cPP and cPPCNs have a broad amorphous background superimposed upon five sharp diffraction lines ascribed to the (110), (040), (130), (111), and (041) planes in order of increasing angles, suggesting that the cPP and the

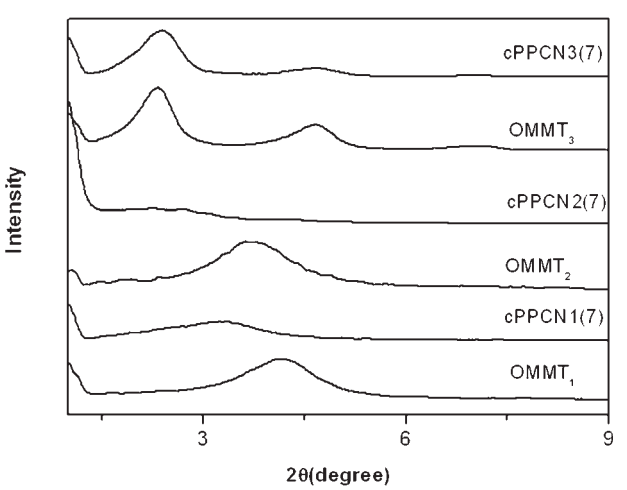

Figure 2 WAXD patterns for three pure organoclays and their cPP–clay composites with 7 wt % clay loadings.

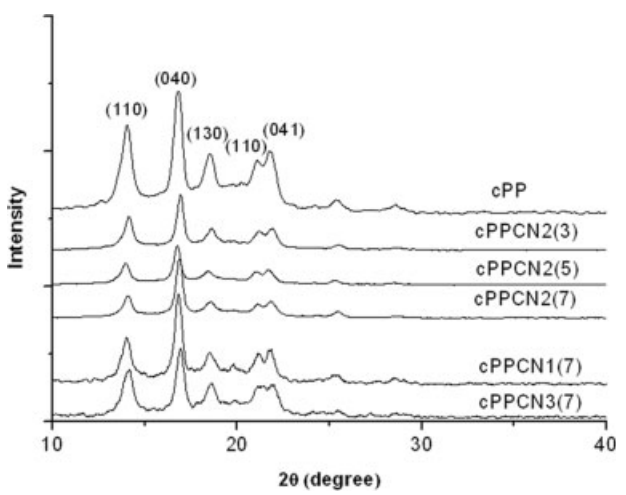

Figure 3 X-ray diffraction results of pure cPP and cPP–clay composites.

cPP–clay composites all crystallize into a monoclinic crystal lattice, typical of α-form.[13–14] Nevertheless, the presence of organoclay has no effect on the polymorphism of cPP crystals in composites, because there are no measurable shifts in the positions of the lines in terms of varying either the $OMMT_2$ loading or the OMMT type. As shown in Figure 3, the intensity corresponding to the diffraction of cPP in different cPPCN samples is considerably lower than that of the pure cPP. Variations in the relative intensities of the diffractions here should be due to the differences in the crystallite size and degree of crystallinity,[15] but which plays the main factor could be clarified by the following thermal analysis by differential scanning calorimetry (DSC). In addition, with the same clay loading of 7 wt %, intensities of the diffractions for cPPCN1(7), cPPCN2(7), and cPPCN3(7) are observed as the following decreasing order of cPPCN1(7) > cPPCN3(7) > cPPCN2(7), which seems to be reversed to the good dispersion order of OMMT layers in cPPCN composites.

The DSC results of all samples are listed in Table III. It is found that the blending of different nanoclay into the cPP matrix did not act nucleating role on the cPP crystallization of cPP composites based on the onset crystallization temperature ($T_{c,onset}$). The peak crystallization temperature ($T_{c,p}$) slightly decreases in cPPCNs, implying that the growth of cPP crystals is slowed down because of the presence of organoclay during crystallization. Moreover, the slightly decreased melting temperature ($T_{m,onset}$ and $T_{m,p}$) of cPP composites indicates a diminishment in the crystallite size and less perfect cPP crystals formed in cPPCNs with 7 wt % contents. Seen from the ΔH_m data in Table III, it can be deduced that the crystallinity of different composites decreases as the clay content increases. The higher ΔH_m of cPPCN2(5) than that of cPPCN2(7), associated with the lower diffraction intensity of cPPCN2(5) than cPPCN2(7) by XRD, suggests that the PP crystals in cPPCN2(5) are smaller but more perfect than in cPPCN2(7),

TABLE III
Results from the DSC Observation

Sample	$T_{c,onset}$ (°C)	$T_{c,p}$ (°C)	$T_{m,onset}$ (°C)	$T_{m,p}$ (°C)	ΔH_m (J/g)
cPP	126.3	123.4	160.2	165.7	89.7
cPPCN0	126.8	122.5	157.8	165.6	92.6
cPPCN2(3)	125.8	122.3	157.5	165.1	86.9
cPPCN2(5)	126.1	122.7	156.6	165.8	81.4
cPPCN2(7)	125.8	122.6	156.5	164.7	73.1
cPPCN1(3)	125.7	122.0	154.5	164.8	93.5
cPPCN1(5)	126.7	122.0	157.0	165.5	82.4
cPPCN1(7)	126.5	122.5	156.9	165.3	75.1
cPPCN3(3)	125.4	121.7	157.0	165.1	80.1
cPPCN5(5)	125.6	122.0	156.7	165.7	74.0
cPPCN3(7)	125.7	121.7	155.2	164.6	71.2

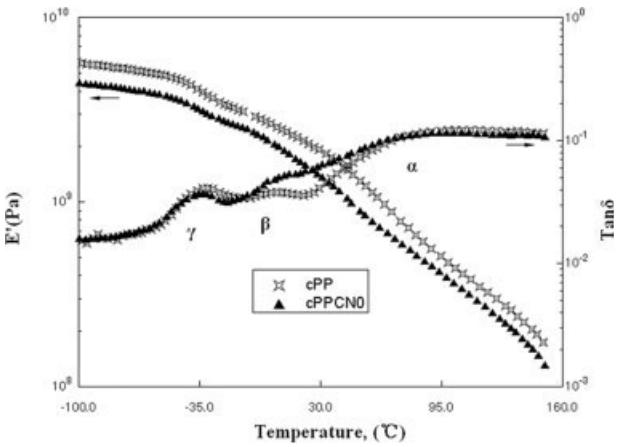

Figure 4 E' and tan δ of neat cPP and cPP/21 wt % MA-PP blend (cPPCN0) as a function of temperature at 1 Hz.

which is consistent with the better dispersion of $OMMT_2$ layers in cPPCN2(5) than in cPPCN2(7). In addition, at the same clay loadings, the lower ΔH_m of cPP-$OMMT_3$ systems than that of two other cPP–clay systems implies less perfect PP crystals in cPP-$OMMT_3$ systems.

Transitions and relaxations

Effects of the MA-PP compatibilizer

The mechanical relaxation spectrum (the storage tensile modulus E' and loss tangent tan δ over a wide temperature range at 1 Hz) for pure cPP and cPPCN0 are depicted in Figure 4. Simultaneously, the variations on the temperature location and activation energy of polymer relaxations, representing the dynamic responses of samples, are compiled and listed in Table IV.

As seen in Figure 4, the tan δ curve of pure cPP exhibits three transition peaks in the vicinity of 103.8, 5.4, and −32.3°C, corresponding to α, β, and γ relaxations, respectively. The weak α-relaxation, universally observed in all crystalline polymers, is assigned to the motion of cPP molecular chains within the crystalline regions. The dominant β-relaxation, corresponding to the glass-rubber transition of the amorphous portion of cPP, is designated as the movement of cPP segments, and the peak temperature of this relaxation process is the glass transition temperature (T_g). Lastly, the γ-relaxation located at about −32.3°C should be associated with the segmental motion of ethylene sequence in the amorphous regions, because this relaxation is not observed in homo-polypropylene.[16–19]

The addition of MA-PP compatibilizer into cPP caused the decrease of E' for the corresponding blend (cPPCN0), as evidenced from Figure 4. Nonetheless, the MA-PP effect on three cPP relaxations should be analyzed separately as follows in order of decreasing

TABLE IV
Peak Temperature and Activation Energy of cPP Different Relaxations in All Samples

Material	$T_{\alpha,\ peak}$ (°C), 1 Hz	$\Delta E_{a,\alpha}$ (kJ/mol)	$T_{\beta,peak}$ (°C), 1 Hz	$\Delta E_{a,\beta}$ (kJ/mol)	$T_{\gamma,peak}$ (°C), 1 Hz	$\Delta E_{a,\gamma}$ (kJ/mol)
cPP	103.8	142.0	5.4	510.7	−32.3	308.5
cPPCN0	101.3	138.7	4.7	361.2	−33.8	263.4
cPPCN2(3)	106.8	183.4	10.8	426.3	−33.4	296.4
cPPCN2(5)	104.0	143.6	8.3	373.9	−32.6	299.7
cPPCN2(7)	99.1	112.2	8.2	305.2	−33.0	339.6
cPPCN1(3)	105.9	163.4	11.6	462.9	−34.6	262.3
cPPCN1(5)	102.8	137.9	9.9	432.1	−31.1	287.5
cPPCN1(7)	96.6	108.0	6.9	191.2	−35.2	232.3
cPPCN3(3)	95.2	128.9	10.0	389.4	−34.1	265.0
cPPCN3(5)	88.7	119.5	8.2	328.0	−32.6	294.5
cPPCN3(7)	86.5	106.5	7.2	287.2	−33.7	331.8

temperature. As seen in Figure 4 and Table IV, the α-relaxation peak of cPPCN0 displays little difference from that of pure cPP, associated with almost the same loss tangent tan δ, location temperature, and relaxation activation energy for this transition process, which indicates of similar crystalline characteristic in cPPCN0 and cPP. However, the addition of MA-PP has great effect on the dominant β-relaxation of the amorphous portions of cPPCN0. The β-transition of cPPCN0 exhibits broader peak, lower β-peak temperature, and higher loss tangent tan δ compared with that of cPP; moreover, the activation energy of this β-process greatly decreases. These results suggest a greater amorphous content and a higher mobility of polymer segments in cPPCN0. In addition, a slightly lower temperature of the γ-relaxation and a small decrease in the activation energy are observed in cPPCN0, directly related to the reduction of the cPP content in cPPCN0, as seen in Table IV. As mentioned earlier, it could be deduced that the MA-PP addition led to high glass-rubber transition content of the corresponding composite.

Effects of clay loadings

As the other two cPP-OMMT systems (cPP-OMMT1 and cPP-OMMT3) display the same dynamic performance as the cPP-OMMT2 system when the OMMT increases, the cPP-OMMT2 system is as a typical example in discussion of the clay loading effect. Figure 5 merely shows the plots of the storage modulus versus temperature of cPP-$OMMT_2$ systems with different $OMMT_2$ loadings. As shown in Figure 5, the storage modulus (E') of cPP-$OMMT_2$ composites does not monotonically increase with clay loadings. cPPCN2(5) displays a maximal E' in the whole temperature region, considerably offsetting the E' decrease as a result of the compatibilizer added in different composites. Therefore, it could be concluded that the addition of 5 wt % $OMMT_2$ is an optimum content for the strength enhancement of cPP composites, correlated with the good perfection of cPP crystals in the composite. Similar result could be also observed in cPP-OMMT1 and cPP-OMMT3 systems.

The effect of clay loadings on transitions and relaxations of polymer in cPP-$OMMT_2$ systems is shown in the form of loss tangent in Figure 6. As seen in Figure 6(a) and Table IV, compared with the cPPCN0, the α-relaxation shifts to a higher temperature associated with higher activation energy for cPP-$OMMT_2$ composites when less than 5 wt % $OMMT_2$ added. Subsequently, a reduction of the α-relaxation temperature and activation energy is observed for the cPP-$OMMT_2$ composite with 7 wt % $OMMT_2$. These results reflect that small addition of $OMMT_2$ could give rise to strong restrictions on the movement of polymer chains in composites, but this restriction decreases as the $OMMT_2$ content further increases above 5 wt %. These results are somewhat in agreement with the previous analysis of less perfect cPP crystals formed in composites with the clay addition increasing. In addition, the damping factor

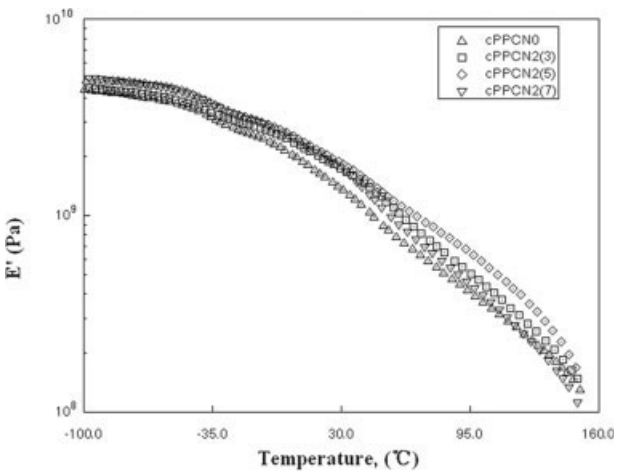

Figure 5 The temperature dependence of E' for cPP composites with different $OMMT_2$ contents at 1 Hz.

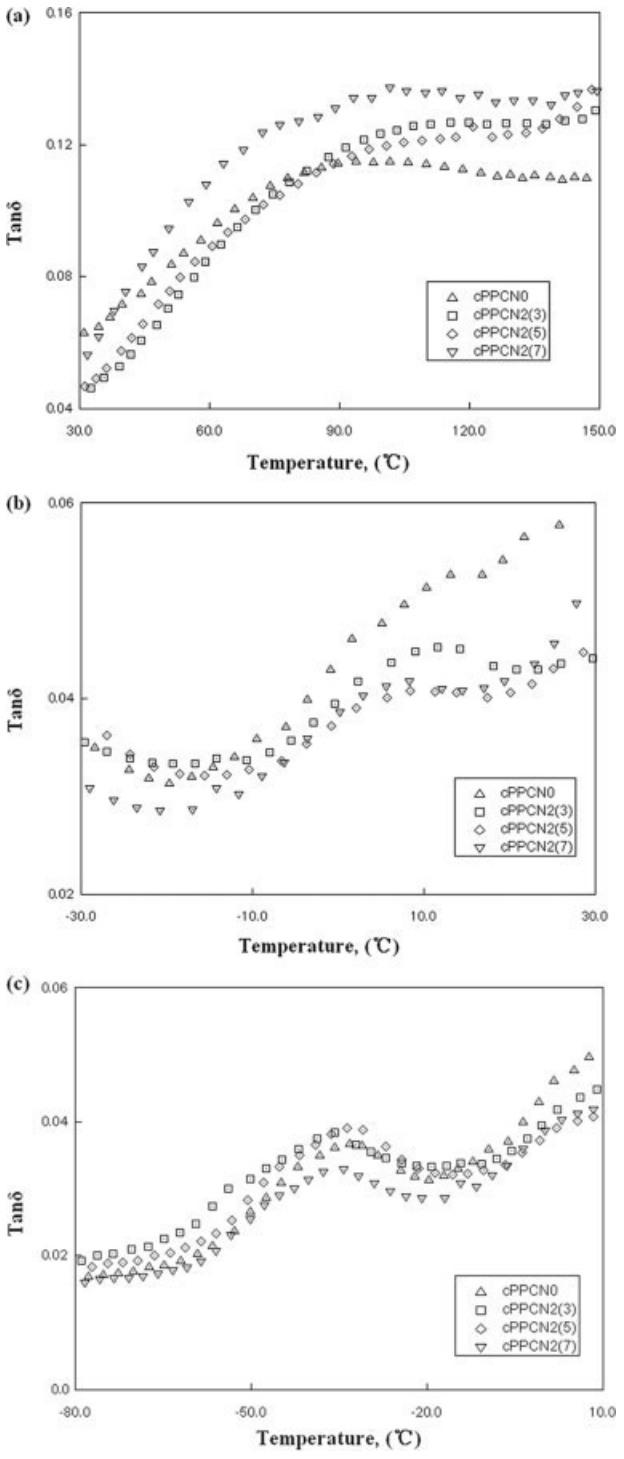

Figure 6 The temperature dependence of tan δ for cPP composites with different OMMT2 contents at 1 Hz: (a) the α transition region; (b) the β transition region; (c) the γ transition region.

(tan δ) of the α-relaxation for cPP-$OMMT_2$ systems is always higher than that for the cPP matrix. The broader α-peak and higher tan δ of cPPCN2(7) than that of cPPCN2(3) and cPPCN(5) further confirms the lower crystallinity and less perfection of cPP crystals in cPPCN2(7).

As seen in Figure 6(b), the dominant β-relaxation of cPP in cPPCN2 samples exhibits distinct differences with respect to the matrix cPP. The tan δ of the β-relaxation for different composites is apparently lower than the matrix, different from the above α-relaxation. The tan δ drops to the lowest value at 5 wt % $OMMT_2$ content. The β-peak shifts to a higher temperature and trends to be more evident due to the presence of $OMMT_2$. Furthermore, the restriction of $OMMT_2$ on the β-relaxation behavior decreases with $OMMT_2$ content increasing, according to the activation energy order of $\Delta E_{a,\beta}$(cPPCN2(3)) > $\Delta E_{a,\beta}$(cPPCN2(5)) > $\Delta E_{a,\beta}$(cPPCN0) > $\Delta E_{a,\beta}$(cPPCN2(7)) in Table IV. From these results, it could be known that the addition of about 3–5 wt % $OMMT_2$ loadings, obviously causes a constrained amorphous phase, in which the PP segmental motions are strongly depressed; however, such this constraint is deeply dispelled when 7 wt % OMMT2 is added. In the amorphous phase, the constraints imposed on the segmental motions originate from several sources such as tie molecules, loose loops, spatial restrictions imposed by surrounding crystalline phases and internal strains in the amorphous chains themselves, among which spatial restriction imposed by the surrounding crystalline phases is the main cause of the constraints.[19–20] The stronger restriction on the β-relaxation of cPP in cPPCN2(3) and cPPCN(5), than in cPPCN2(7), is in good agreement with the more perfect cPP crystals existed in cPPCN2(3) and cPPCN(5) directly correlated with the better dispersion of clay layers. It is evident that the β-relaxation for cPPCN2 systems intensifies with the perfection of cPP crystals increasing in cPPCN composites.

The γ-relaxation peak of cPP only slightly changes in height but hardly in temperature for cPPCN2 composites with varying $OMMT_2$ content, as seen in Figure 6(c). Compared with the cPPCN0, the activation energy of the γ-process ($\Delta E_{a,\gamma}$) slightly increases with the $OMMT_2$ content increasing, according to the datum in Table IV. The cPPCN2(7) displays higher $\Delta E_{a,\gamma}$ and lower tan δ than the two other cPPCN2 composites. From these results, it could be deduced that the increase of clay loadings within the cPP matrix would cause stronger constraints on the γ-relaxation of cPP, which will directly impair the good impact strength of cPP.

Effect of the clay pretreatment history

The variations resulting from the clay different pretreatments on the transitions and relaxations of cPP in composites are also listed in Table IV. Though these three types of clay are pretreated with different organomodifiers, their effects on the α-relaxation of cPPCN composites show similar tendency, referred to the values of $T_{\alpha,\text{peak}}$ and $\Delta E_{a,\alpha}$ in Table IV. $T_{\alpha,\text{peak}}$ and $\Delta E_{a,\alpha}$

for different cPP–clay composites decrease with the clay loading increasing. However, with the same clay loading, the value order of $T_{\alpha,peak}(OMMT_2) > T_{\alpha,peak}(OMMT_1) > T_{\alpha,peak}(OMMT_3)$ and $\Delta E_{a\prime\alpha}(OMMT_2) > \Delta E_{a\prime\alpha}(OMMT_1) > \Delta E_{a\prime\alpha}(OMMT_3)$ for different composites represents the perfection order of cPP crystals in these cPPCNs. The cPP crystals are more perfect in cPP-$OMMT_2$ systems than in the two other cPP–clay systems, which is in agreement with the structure analysis by DSC.

Effects of the clay types on the β-relaxation for different composites is similar to each other by varying their loadings, according to the variations of $T_{\beta,peak}$ and $\Delta E_{a\prime\beta}$ in Table IV. The increased $T_{\beta,peak}$ and $\Delta E_{a\prime\beta}$ for different composites decreases with the clay loading increasing. However, with same clay content, the β-relaxation of cPP in composites displays some differences due to the different clay pretreatment history. With 3–5 wt % loadings, the cPP-$OMMT_1$ and cPP-$OMMT_2$ systems display higher $T_{\beta,peak}$ and $\Delta E_{a\prime\beta}$ than cPP-$OMMT_3$ systems, consistent with the higher crystallinity of cPP-$OMMT_1$ and cPP-$OMMT_2$ systems by DSC results. This result indicates that the β-relaxations for different composites, assigned to the motions of cPP chain segments in amorphous portions, are related to the crystalline structure of composites. The stronger constraints on the β-relaxation by $OMMT_1$ and $OMMT_2$ than by $OMMT_3$, implies the higher affinity of cPP and $OMMT_1$ or $OMMT_2$ than that of cPP and $OMMT_3$. When clay layers appear jam effect within the matrix with 7 wt % content, the value order of $T_{\beta,peak}$(cPPCN2(7)) > $T_{\beta,peak}$(cPPCN3(7)) > $T_{\beta,peak}$(cPPCN1(7)) and $\Delta E_{a,\beta}$(cPPCN2(7)) > $\Delta E_{a,\beta}$(cPPCN3(7)) > $\Delta E_{a\prime\beta}$(cPPCN1(7)) agrees well with the previous dispersion order of $OMMT_2 > OMMT_3 > OMMT_1$ within the matrix.

As shown in Table IV, the γ-relaxations of cPP in different composites hardly changes when the clay type varies, which suggests that the motion of ethylene sequence of cPP is insensitive to the clay pretreatment.

CONCLUSIONS

In this study, effects of the clay loading and pretreatment history on the transitions and relaxations of cPP molecules in different cPPCNs were carefully detected, associated with the structure analysis for these composites. The clay displays increasing stacks status of layers in different cPP–clay composites with increasing clay content. At the same clay loading, $OMMT_2$ pretreated with $C_{18}H_{37}N(CH_3)_3^+$ could be more exfoliated into the cPP matrix than $OMMT_1$ modified by $C_{18}H_{37}NH_3^+$, while $OMMT_3$ modified by $(C_{18}H_{37})_2N(CH_3)_2^+$ almost remains its original structure within the composite. The addition of different clays has no effect on the polymorphism of cPP crystals in different composites, only leads to a diminishment in the cPP crystal size and perfection as the clay loading increases. Transitions and relaxations of cPP molecular units in different cPPCNs show that the α-relaxation, assigned to the motion of polymer chains within the crystalline regions of different cPPCNs, is activated with clay content increasing, owing to the less perfect cPP crystals formed in composites. The dominant β-relaxation in cPPCNs, corresponding to the movement of PP segments within the amorphous portions of cPPCNs, is greatly limited with the clay addition of 3–5 wt %, whereas facilitated by 7 wt % clay loading due to the increasing inhomogeneous dispersion of clay layers within the composite. Lastly, the γ-relaxation of cPP, associated with the segmental motion of ethylene sequence of cPP chains, is restricted with clay content increasing. Additionally, it is known that the intercalation of cPP into interlayer spaces of $OMMT_3$ decreases due to the obstruction of the $2C_{18}$-chains congested between interlayers of $OMMT_3$.

References

1. Kurokawa, Y.; Yasuda, H.; Oya, A. J Mater Sci Lett 1996, 15, 1481.
2. Ding, C.; Jia, D. M.; He, H.; Guo, B. C.; Hong, H. Q. Polym Test 2005, 24, 94.
3. Manias, E.; Touny, A.; Wu, L.; Strawhecker, K.; Lu, B.; Chung, T. C. Chem Mater 2001, 13, 3516.
4. Leuteritz, B. A.; Pospiech, D.; Kretzschmar, B.; Willeke, M.; Jehnichen, D.; Jentzsch, U.; Grundke, K.; Janke, A. Adv Eng Mater 2003, 5, 678.
5. García-López, D.; Picazo, O.; Merino, J. C.; Pastor, J. M. Eur Polym J 2003, 39, 945.
6. Koo, C. M.; Kim, J. H.; Wang, K. H.; Chung, I. J. J Polym Sci Part B: Polym Phys 2005, 43, 158.
7. Reichert, P.; Nitz, H.; Klinle, S. Macro Mater Eng 2000, 275, 8.
8. Chiu, F. C.; Lai, S. M.; Chen, J. W.; Chu, P. H. J Polym Sci Part B: Polym Phys 2004, 42, 4139.
9. López-Manchado, M. A.; Arroyo, M. Polymer 2000, 41, 7761.
10. Ward, I. M. Mechanical Properties of Solid Polymers; Wiley Interscience: London, 1971.
11. Amash, A.; Zugenmaier, P. J Appl Polym Sci 1997, 63, 1143.
12. Heijboar, J. In Molecular Basis of Transitions and Relaxations; Meier, D. J., Ed.; Gordon and Breach Science Publishers: New York, 1978; p 75.
13. Zheng, W. G.; Lu, X. H.; Toh, C. L.; Zheng, T. H.; He, C. B. J Polym Sci Part B: Polym Phys 2004, 42, 1810.
14. Lovinger, A. J.; Chua, J. O.; Gryte, C. C. J Polym Sci Polym Phys Ed 1977, 15, 641.
15. Isasi, J. R.; Alamo, R. G.; Mandelkern, L. J Polym Sci Part B: Polym Phys 1997, 35, 2511.
16. Nitta, K.-H.; Tanaka, A. Polymer 2001, 42, 1219.
17. Mansfield, M.; Boyd, R. H. J Polym Sci Polym Phys Ed 1978, 16, 1227.
18. Boyd, R. H. Polymer 1985, 26, 1123.
19. Feng, Y.; Jin, X.; Hay, N. J Appl Polym Sci 1998, 68, 395.
20. Inamura, I.; Yamamura, H. J Polym Sci Part B: Polym Phys 1976, 14, 1221.